Pulsed oxidation and biological evolution in the Ediacaran Doushantuo Formation

Kathleen A. McFadden*, Jing Huang†, Xuelei Chu†‡, Ganqing Jiang‡§, Alan J. Kaufman‡¶, Chuanming Zhou‖, Xunlai Yuan‖, and Shuhai Xiao*‡

*Department of Geosciences, Virginia Polytechnic Institute and State University, Blacksburg, VA 24061; †Key Laboratory of Mineral Resources, Institute of Geology and Geophysics, Chinese Academy of Sciences, Beijing 100029, China; §Department of Geoscience, University of Nevada, Las Vegas, NV 89154; ¶Department of Geology, University of Maryland, College Park, MD 20742; and ‖State Key Laboratory of Palaeobiology and Stratigraphy, Nanjing Institute of Geology and Palaeontology, Chinese Academy of Sciences, Nanjing 210008, China

Edited by Paul F. Hoffman, Harvard University, Cambridge, MA, and approved January 9, 2008 (received for review September 5, 2007)

Recent geochemical data from Oman, Newfoundland, and the western United States suggest that long-term oxidation of Ediacaran oceans resulted in progressive depletion of a large dissolved organic carbon (DOC) reservoir and potentially triggered the radiation of acanthomorphic acritarchs, algae, macroscopic Ediacara organisms, and, subsequently, motile bilaterian animals. However, the hypothesized coupling between ocean oxidation and evolution is contingent on the reliability of continuous geochemical and paleontological data in individual sections and of intercontinental correlations. Here we report high-resolution geochemical data from the fossil-rich Doushantuo Formation (635–551 Ma) in South China that confirm trends from other broadly equivalent sections and highlight key features that have not been observed in most sections or have received little attention. First, samples from the lower Doushantuo Formation are characterized by remarkably stable $\delta^{13}C_{org}$ (carbon isotope composition of organic carbon) values but variable $\delta^{34}S_{CAS}$ (sulfur isotope composition of carbonate-associated sulfate) values, which are consistent with a large isotopically buffered DOC reservoir and relatively low sulfate concentrations. Second, there are three profound negative $\delta^{13}C_{carb}$ (carbon isotope composition of carbonate) excursions in the Ediacaran Period. The negative $\delta^{13}C_{carb}$ excursions in the middle and upper Doushantuo Formation record pulsed oxidation of the deep oceanic DOC reservoir. The oxidation events appear to be coupled with eukaryote diversity in the Doushantuo basin. Comparison with other early Ediacaran basins suggests spatial heterogeneity of eukaryote distribution and redox conditions. We hypothesize that the distribution of early Ediacaran eukaryotes likely tracked redox conditions and that only after ≈551 Ma (when Ediacaran oceans were pervasively oxidized) did evolution of oxygen-requiring taxa reach global distribution.

acritarchs | isotopes | redox | Neoproterozoic | early animals

The Ediacaran (635–542 Ma) Earth witnessed profound changes in the aftermath of widespread and potentially global ice ages, including the evolution and radiation of complex megascopic life and major perturbations of the global carbon cycle that accompanied oxygenation of the deep ocean (1–9). These biological and environmental events have been speculatively linked, yet their temporal relationships have not been accurately documented in relatively continuous and fossil-rich sections that span a range of well-documented depositional settings. For example, geochemical data from siliciclastic-dominated Ediacaran successions in Newfoundland (5) and the western United States (7) are incomplete, and those from the early Ediacaran interval in Oman (4) are of low stratigraphic resolution. Furthermore, paleontological data from these successions are limited to macroscopic Ediacara fossils and the biomineralizing animal *Cloudina* (10).

To further test the proposed linkages between redox changes and biological evolution (4, 5), we carried out a high-resolution chemostratigraphic and biostratigraphic investigation of the fossiliferous Doushantuo Formation in the Yangtze Gorges area, South China. Our data reveal pulsed oxidation events that coincide with the origination and diversification of acanthomorphic acritarchs and other multicellular life forms in the basin. In combination with available data from other Ediacaran successions, our results indicate that oxidation of terminal Proterozoic oceans may have been episodic (4), with the final and permanent oxidation occurring ≈551 Ma.

Sedimentological, Paleontological, and Geochemical Data

The Doushantuo Formation in the Yangtze Gorges area, constrained between 635.2 ± 0.6 and 551.1 ± 0.7 Ma (11), is divided into four lithostratigraphic members (Fig. 1). At the Jiulongwan section [supporting information (SI) Fig. 3], member I represents an ≈5-m-thick cap dolostone overlying the Nantuo glacial diamictite and contains a suite of enigmatic sedimentary structures and textures (12, 13). Member II is characterized by ≈70 m of alternating organic-rich shale and dolostone beds with abundant pea-sized chert nodules. Member III is ≈70 m thick and is composed of dolostone and bedded chert in the lower part that passes up-section into alternating limestone-dolostone "ribbon rocks." Member IV is an ≈10-m-thick black, organic-rich shale unit that is widespread across the Yangtze Gorges area and defines the lithologic boundary between the Doushantuo Formation and the overlying Dengying Formation.

The Doushantuo Formation is widely distributed in South China and was deposited in shelf marine environments on a passive continental margin (*SI Text*). Sedimentological evidence suggests that the entire Doushantuo Formation at Jiulongwan was deposited below or near wave base. There is currently no evidence for subaerial exposure surfaces or erosional unconformities, although unrecognized small-scale hiatuses may exist. Three transgressive-regressive cycles can be identified in the Doushantuo and lower Dengying formations (Fig. 1). Cycle 1 begins with transgression associated with the cap carbonate and deepening in lower member II, followed by regression in upper member II. The regressive trend is indicated by the change from deep subtidal silty dolostone with parallel and wrinkle laminations to shallow subtidal carbonates with small-scale cross-laminations and phosphatic intraclasts. Cycle 2 is not bounded by subaerial exposure surfaces. It starts near the member II/III

Author contributions: X.C., G.J., A.J.K., and S.X. designed research; K.A.M., J.H., X.C., G.J., A.J.K., C.Z., X.Y., and S.X. performed research; X.C., G.J., A.J.K., and S.X. contributed new reagents/analytic tools; K.A.M., J.H., X.C., G.J., A.J.K., C.Z., X.Y., and S.X. analyzed data; and K.A.M., J.H., X.C., G.J., A.J.K., C.Z., X.Y., and S.X. wrote the paper.

The authors declare no conflict of interest.

This article is a PNAS Direct Submission.

‡To whom correspondence may be addressed. E-mail: kaufman@geol.umd.edu, xlchu@mail.igcas.ac.cn, ganqing.jiang@unlv.edu, or xiao@vt.edu.

This article contains supporting information online at www.pnas.org/cgi/content/full/0708336105/DC1.

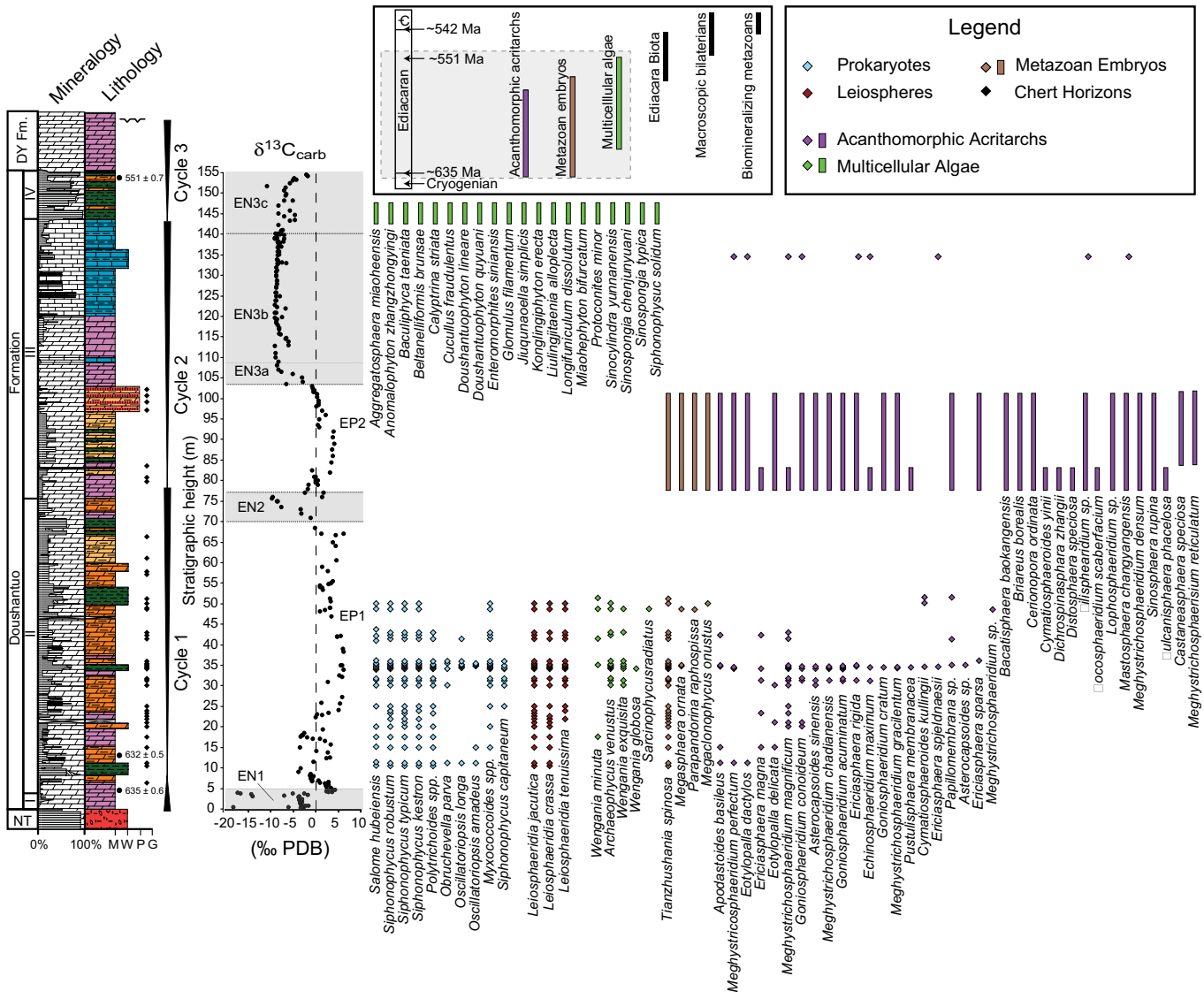

Fig. 1. Fossil distribution in the Doushantuo Formation. Member II fossil occurrences are from the Jiulongwan section, and member III fossil occurrences are from the nearby Tianjiayuanzi section (diamonds) in the Yangtze Gorges and the Weng'an section (bars) in Guizhou Province (6, 38). The member IV fossils are occurrences from the nearby Miaohe section (15). Acanthomorph taxonomy follows that in ref. 22, pending systematic revision of several taxa. Diamonds indicate actual stratigraphic occurrences; bars, stratigraphic ranges based on first and last occurrences. The *Inset* shows generalized fossil distribution in the Ediacaran Period (4, 11), and the shaded portion represents the Doushantuo Formation. See SI Fig. 3 for section localities and Fig. 2 for explanation of stratigraphic column and $\delta^{13}C_{carb}$ features. PDB, PeeDee belemnite. NT, Nantuo Formation; DY, Dengying Formation.

boundary, with laminated black shale and lime mudstones above a transgressive surface. The regressive trend of this cycle is expressed by up-section increase of phosphatic packstone, scour marks, low-angle cross-laminations, and microbial mats. The sharp lithostratigraphic contact between member III and IV represents a transgressive surface and defines the base of cycle 3. This cycle includes deep subtidal black shales of member IV and peritidal dolostones of the lower Dengying Formation containing tepee structures and karstification features.

The Doushantuo Formation is richly fossiliferous. At the Jiulongwan section, complex acanthomorphic acritarchs, probable animal eggs and embryos, multicellular algae, and filamentous and coccoidal cyanobacteria are preserved in early diagenetic chert nodules in member II (Fig. 1). Acanthomorphic acritarchs first appear in basal member II, less than 12 m above the Nantuo diamictite, and their diversity progressively increases in member II. Among the earliest acanthomorphic acritarchs is *Tianzhushania spinosa*, a species that was recently interpreted as representing animal embryos with a diapause stage (8, 14). Because of taphonomic issues (6), biostratigraphic data must be integrated from multiple sections that can be confidently correlated with the Jiulongwan section. Paleontological data from the nearby Tianjiayuanzi and Xiaofenghe sections (SI Fig. 3) indicate that acanthomorphic acritarchs continue to diversify in member III, but in all examined sections they are restricted to members II and III (6, 8). Member IV at the Miaohe section contains more than 20 species of macroscopic carbonaceous compression fossils, most of which are likely macroalgal fossils (15), although a few may represent animals (16); one of these macroalgal fossils, *Enteromorphites siniansis* (a dichotomous thallus), also occurs in member II at Jiulongwan (17). The overlying Dengying Formation yields frondose and fractal Ediacara fossils (18, 19), horizontal trace fossils made by bilaterian animals (20), and biomineralizing tubular animals (21).

At Weng'an ≈750 km to the southwest, the upper Doushantuo Formation, traditionally correlated with member III in the

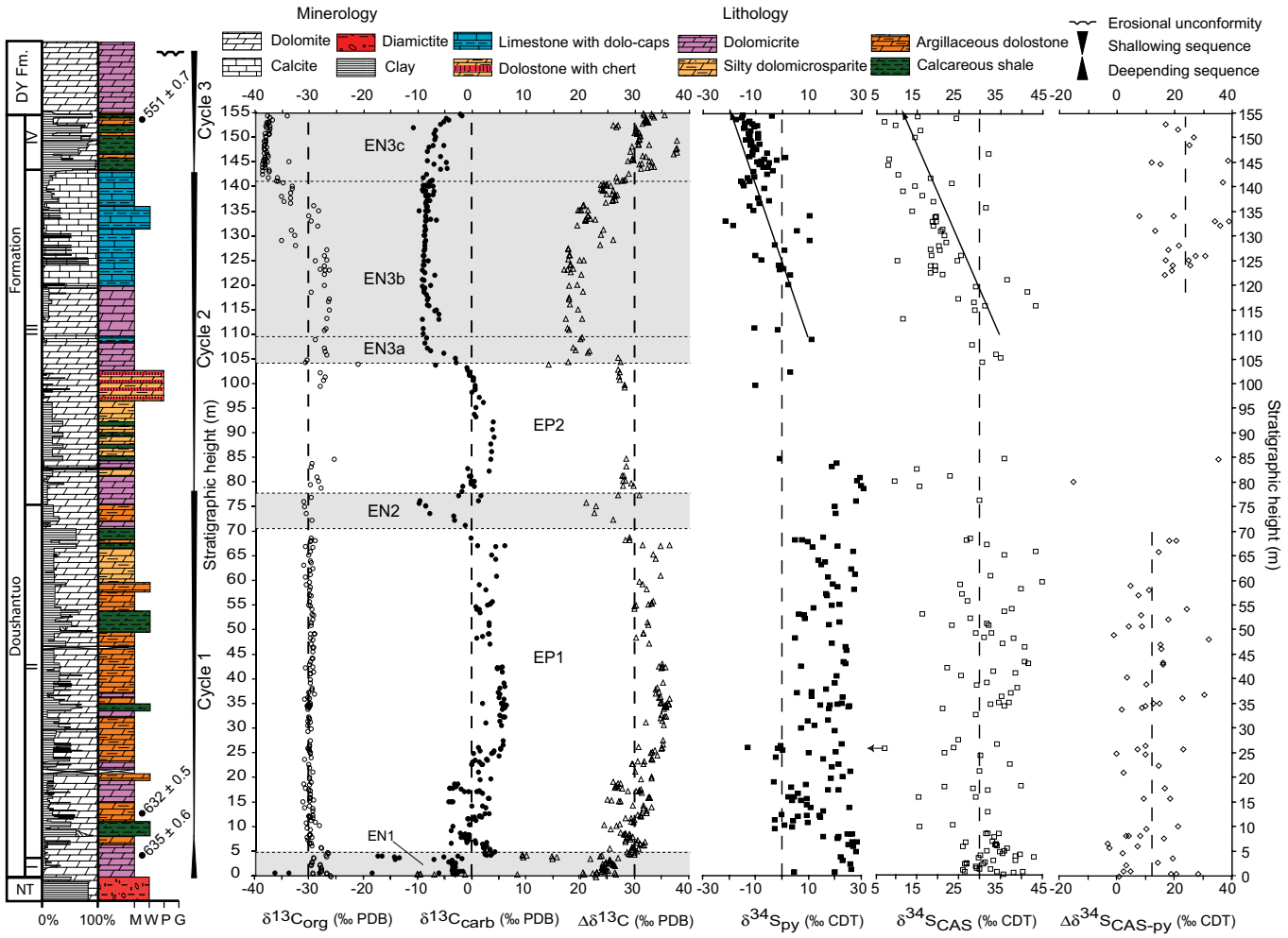

Fig. 2. Chemostratigraphic profiles of the Doushantuo Formation at Jiulongwan. The lithostratigraphic division (I–IV), sedimentary cycles (1–3), and $\delta^{13}C_{carb}$ features (EN1, EP1, EN2, EP2, EN3a, EN3b, and EN3c) are labeled. The left edge of the stratigraphic column shows percentages of dominant mineralogy (calcite vs. dolomite vs. terrigenous clay) estimated from thin sections, and the right edge shows dominant lithologies. M, micrite; W, wackestone; P, packstone; G, grainstone; NT, Nantuo Formation; DY, Dengying Formation.

Yangtze Gorges area (22), contains exceptionally preserved cyanobacteria, acanthomorphic acritarchs, animal embryos, and multicellular algae that are taxonomically similar to those from members II and III in the Yangtze Gorges area (6, 22).

To evaluate temporal changes in seawater chemistry, we measured carbon and sulfur isotope compositions in both reduced (organic matter and pyrite) and oxidized (carbonate and trace sulfate) phases at high stratigraphic resolution in the Doushantuo Formation at Jiulongwan (Fig. 2; see *Methods* and *SI Text* and SI Fig. 7 for diagenetic evaluation). The carbon isotope composition of carbonate ($\delta^{13}C_{carb}$) shows three prominent negative excursions (EN1–EN3) separated by generally positive values (EP1 and EP2), consistent with $\delta^{13}C_{carb}$ data from other sections in the Yangtze Gorges area (23). In contrast, the carbon isotope composition of organic carbon ($\delta^{13}C_{org}$) is remarkably stable in member II [with values of approximately −30 per mil (‰)], increases slightly to −27‰ in member III, and decreases significantly to −38‰ in member IV. $\Delta\delta^{13}C_{carb\text{-}org}$ is largely between 25‰ and 37‰ in the Doushantuo Formation but decreases to 16–20‰ in association with both negative $\delta^{13}C_{carb}$ excursions (EN2 and lower EN3). Sulfur isotopes show greater variation than carbon isotopes, particularly in members I and II, where the sulfur isotope composition of pyrite ($\delta^{34}S_{py}$) and carbonate-associated sulfate ($\delta^{34}S_{CAS}$) show ≈30‰ variations without persistent stratigraphic trend. Some stratigraphic variation in $\delta^{34}S_{CAS}$ could be an artifact of pyrite oxidation during sample preparation of pyrite-rich and CAS-poor samples (24). However, cross-plots of geochemical data do not support significant laboratory contamination of $\delta^{34}S_{CAS}$ data (*SI Text* and SI Fig. 7). In upper member III and member IV, both $\delta^{34}S_{CAS}$ and $\delta^{34}S_{py}$ show a distinct negative trend concurrent with the negative $\delta^{13}C_{carb}$ excursion in EN3. $\Delta\delta^{34}S_{CAS\text{-}py}$ values are mostly between 0‰ and 40‰ but are statistically higher in the upper part (mean = 23‰; SD = 9‰) than in the lower part (mean = 11‰; SD = 10‰) of the formation.

Interpretation

Interpretation of the carbon isotope data requires an appreciation of the depositional environment of the Doushantuo sediments, which accumulated below or near wave base. Micritic carbonate in the Doushantuo Formation (as in modern oceans) was likely precipitated from the surface water, whereas organic carbon may have integrated biosynthesis throughout the water column. The Doushantuo carbon isotope data can be interpreted in terms of a non-steady-state carbon cycle involving a large dissolved organic carbon (DOC) reservoir (25). We suggest that the bulk of the DOC pool lay below an oxygen chemocline, suggesting strong redox stratification of Doushantuo seawater. A

large DOC reservoir would buffer the organic carbon isotopic value of seawater and that of sedimentary organic matter derived from DOC through bacterial scavenging and recycling. This scenario is consistent with the remarkably constant $\delta^{13}C_{org}$ values in member II, a feature not previously recognized in other Ediacaran successions. In contrast, variable and generally positive $\delta^{13}C_{carb}$ values in member II (EP1) and lower member III (EP2) may reflect a combination of factors (e.g., increased carbon fixation, fractionation factor, and $\delta^{13}C$ value of weathering input) interacting with a comparatively small dissolved inorganic carbon (DIC) reservoir in the surface water. The isotopic difference between carbonate and organic carbon ($\Delta\delta^{13}C_{carb\text{-}org}$) in member II is greater than isotopic fractionation associated with Calvin cycle carbon fixation. However, because the DIC and DOC reservoirs were likely decoupled, the record of $\Delta\delta^{13}C_{carb\text{-}org}$ variation largely reflects perturbations of the DIC pool alone.

The negative $\delta^{13}C_{carb}$ excursions (EN1–EN3) are interpreted in terms of significant perturbations to the DIC reservoir. The biogeochemical anomaly in the cap carbonate (EN1) has been interpreted as evidence for gas-hydrate destabilization during postglacial warming (26), although additional tests are required to evaluate alternative hypotheses (2, 7, 27, 28). The negative $\delta^{13}C_{carb}$ excursion EN2 has been identified in several sections in the Yangtze Gorges area (23, 29, 30). However, two previous chemostratigraphic studies in this region failed to recover this isotopic anomaly because of poor stratigraphic resolution (31, 32). EN2 was interpreted previously as genetically related to the ≈580-Ma Gaskiers glaciation (11), but this interpretation is inconsistent with the 599 ± 4 Ma Pb–Pb age from the upper Doushantuo Formation (above EN2) at Weng'an (33). In the absence of Ediacaran glacial deposits in South China and in light of apparent decoupling of DOC and DIC reservoirs, the EN2 anomaly is interpreted here as evidence for episodic oxidation of the large DOC reservoir in the anoxic deep ocean (25).

Ediacaran oxidation of the DOC pool likely occurred near the chemocline where the resulting isotopically light DIC was incorporated in the surface ocean, contributing to the negative $\delta^{13}C_{carb}$ values recorded in micritic carbonates. The oxidation was likely driven by enhanced bacteria sulfate reduction ($SO_4^{2-} + 2CH_2O \rightarrow H_2S + 2HCO_3^-$) in response to pulsed increases in seawater sulfate. Oceanic sulfate levels were probably low in early Doushantuo time, as evidenced by meter-scale variations in $\delta^{34}S_{CAS}$ and $\delta^{34}S_{py}$ values in member II (34, 35). However, regression during sedimentary cycle 1, together with increasing atmospheric oxygen levels, may have accelerated oxidative weathering intensity (7), thus increasing sulfate and alkalinity supply to the surface ocean, deepening the chemocline, and leading to partial oxidation of the DOC reservoir and negative $\delta^{13}C_{carb}$ excursion EN2. The amount of sulfate required to account for EN2 is difficult to constrain because of uncertainties in EN2 duration and DIC reservoir size in the surface ocean. Nonetheless, because $\delta^{13}C_{org}$ remains invariant across EN2, the size of the DOC pool was not significantly reduced at this time.

A similar environmental scenario may be applied to the EN3 carbon isotope excursion, which is more pronounced and where $\delta^{13}C_{org}$ values become more variable. In EN3, the shift to negative $\delta^{13}C_{carb}$ values (EN3a) is as rapid as that in EN2 but continues for a significant stratigraphic interval (EN3b). We interpret these observations to be consistent with the strong reduction in the size of the DOC reservoir. The oxidation of DOC was likely driven by the continuous supply of sulfate from oxidative weathering of sulfides during the regression of sedimentary cycle 2. It is notable that both $\delta^{34}S_{CAS}$ and $\delta^{34}S_{py}$ values persistently decrease in EN3a and EN3b, whereas $\Delta\delta^{34}S_{CAS\text{-}py}$ becomes greater than that in member II. These patterns indicate accelerated input of ^{34}S-depleted sulfate to the surface ocean (caused by an increased fraction of sulfide weathering), greater sulfate availability, or increased fractional burial rate of sulfate. These interpretations are consistent with an inferred oxidation event.

The final phase of the upper Doushantuo negative $\delta^{13}C_{carb}$ excursion (EN3c) corresponds to rapid transgression of sedimentary cycle 3 and extremely negative $\delta^{13}C_{org}$ values (−38‰) in member IV. Carbon isotope data from slope and basinal facies (300–600 km south of the Yangtze Gorges area) suggest a strong (up to 10‰) depth gradient in $\delta^{13}C$ of DIC in much of the Doushantuo Formation (30). Upwelling of anoxic and ^{13}C-depleted alkalinity in deep water associated with transgression likely introduced additional ^{13}C-depleted DIC to the surface water and may have caused anoxia or euxinia in the lower photic zone during the deposition of member IV (36). Primary production built on ^{13}C-depleted DIC may have led to the unusually negative $\delta^{13}C_{org}$ values, particularly as the DOC pool waned. Upwelling would also introduce ^{34}S-depleted deep-water sulfides (37) to the surface water, leading to lower $\delta^{34}S_{py}$ and $\delta^{34}S_{CAS}$ values in EN3c. Thus, the isotopic data from EN3 suggest that the DOC reservoir became isotopically more responsive to primary bioproductivity and carbon cycling as its size progressively declined toward the end of the Doushantuo Formation ≈551 Ma. After the negative excursion EN3, $\delta^{13}C_{carb}$ returns to positive values for the entire Dengying Formation in the Yangtze Gorges area (23).

Integration of biostratigraphic and chemostratigraphic data (Figs. 1 and 2) suggests that the oxidation events played a role in controlling the stratigraphic distribution of Doushantuo organisms. At Jiulongwan, the occurrences of microfossils including cyanobacteria, acanthomorphic acritarchs, multicellular microalgae, and probable animal embryos correspond to the $\delta^{13}C_{carb}$ feature EP1. However, inference of evolutionary patterns on the basis of a single section is often biased by the vagaries of fossil preservation and ecological distribution. Integration of paleontological data from other sections in the Yangtze Gorges (6, 8) and Weng'an areas (6, 38) indicates that acanthomorphic acritarchs and animal embryos emerged immediately after EN1 and show a pronounced diversification after the first oxidation event (EN2). It is possible, but unproven at present, that the characteristic acanthomorphs might have gone extinct before the second oxidation event EN3. A radiation of macroscopic algae and possible metazoans (15, 16) occurred at the end of EN3, followed by the appearance of frondose and fractal Ediacaran organisms (18, 19), motile bilaterian animals evidenced by trace fossils (20), and biomineralizing animals (*Cloudina* and *Sinotubulites*) (21, 39). Thus, biological evolution and oceanic oxygenation appear to be closely coupled in the Doushantuo and Dengying formations, although the mechanisms and processes underlying the temporal couplings remain elusive.

Discussion

Considered with previously published data from elsewhere (4–7), geochemical and paleontological data reported here provide a more detailed picture of the Ediacaran environmental and biological evolution. The Doushantuo data reveal important information not preserved in other Ediacaran successions. First, the existence of two discrete negative $\delta^{13}C_{carb}$ excursions (EN2 and EN3) finds equivalents only in the Infra Krol Formation of the Lesser Himalaya (40) and possibly the western United States (7, 41). Close isotopic similarities between South China and Lesser Himalaya are not surprising given the paleogeographic proximity (42). The absence of EN2 equivalents in Oman and South Australia, if EN3 is correlated with the Shuram and Wonoka negative $\delta^{13}C_{carb}$ excursions (11, 43), is likely because of poor stratigraphic resolution and inappropriate lithologies for $\delta^{13}C_{carb}$ analysis in these lower Ediacaran successions (4, 43, 44).

It is also possible that the oxidation event represented by EN2 was temporally short-lived and only expressed locally. Second, the remarkably stable $\delta^{13}C_{org}$ values decoupled from variable $\delta^{13}C_{carb}$ values in Doushantuo member II, representing ≈50 million years if EN2 is of Gaskiers age (11) or <30 million years if we accept the 599 ± 4 Ma age from the upper Doushantuo (33), is strong evidence for a large, isotopically buffered DOC reservoir in the early Ediacaran Period. Such stable $\delta^{13}C_{org}$ values have not been previously reported from other early Ediacaran basins to our knowledge, arguably with the exception of the Masirah Bay and Khufai formations in Oman (4). Third, the high meter-scale variability in $\delta^{34}S_{CAS}$ and $\delta^{34}S_{py}$, particularly in the lower Doushantuo Formation, is distinct from the well defined stratigraphic trends in Oman (4), although the decreasing $\delta^{34}S_{py}$ trend in EN3 seems to be comparable to a similar $\delta^{34}S_{py}$ trend in the Shuram and Buah formations of Oman. However, we note that rapid stratigraphic variations in $\delta^{34}S_{py}$ have been reported from Ediacaran successions in Newfoundland, Australia, and the western United States (5, 7, 35, 45). More data are needed to clarify the global picture of Ediacaran sulfur isotopes, but the apparent spatial heterogeneity of $\delta^{34}S_{CAS}$ and $\delta^{34}S_{py}$ seems to indicate generally low sulfate concentrations in Ediacaran basins where sulfur isotopes are susceptible to local perturbations.

Nevertheless, the Doushantuo data do share several features with other Ediacaran successions. Available geochronological data indicate that Doushantuo EN3 may be correlated with the Shuram negative $\delta^{13}C_{carb}$ excursion in Oman (4), the Wonoka negative excursion in South Australia (46), and the Johnnie negative excursion in western United States (7, 41). However, given the recognition of three pre-550-Ma negative carbon isotope anomalies in the Ediacaran Period, we acknowledge that alternative correlations are possible. At present, the key uncertainty is the temporal relationship between EN2 and the Gaskiers glaciation. Regardless, the decoupled $\delta^{13}C_{carb}$ and $\delta^{13}C_{org}$ trends seen in EN3 are also evident in the Shuram and Wonoka negative excursions (4, 46), indicating that the global surface ocean DIC reservoir may have been disturbed by the oxidation of a large DOC reservoir. This interpretation is also consistent with the generally decreasing trend of $\delta^{34}S_{py}$ reported from South China and Oman (4), suggesting that the fractional flux of sulfide weathering and/or fractional burial of sulfate increased during EN3. In light of increasing $^{87}Sr/^{86}Sr$ values in the Ediacaran (1, 47), it is possible (although inconclusive given the multiple factors controlling S and Sr isotopes) that oxidative weathering of sulfides may have been a global source of ^{34}S-depleted sulfur, which drove the remineralization of DOC, negative $\delta^{13}C_{carb}$ excursion, and decoupled $\delta^{13}C_{carb}$ and $\delta^{13}C_{org}$ trends (7). Thus, we interpret the oxidation event recorded by EN3 as a profound and global event that may have led to permanent oxidation of Ediacaran oceans.

Overall increase in taxonomic diversity and biological complexity as seen in the Doushantuo Formation of South China is consistent with the important role of oxidation events in biological evolution. However, the Ediacaran Period can be envisioned as a protracted transition from a DOC-dominated to a DIC-dominated carbon system, and oxidation of the large DOC reservoir was likely episodic, initiated regionally, and culminated in a global and permanent oxidation of the deep ocean. Thus, during the early phase of this transitional period, redox conditions may have fluctuated and differed between basins. The geographic and stratigraphic distribution of oxygen-requiring organisms may have tracked local redox conditions; for example, the first appearance of some acanthomorphic acritarch genera in South China may predate their appearance in South Australia by as much as 50 million years (6, 48). Only after the final oxidation event (EN3) did biomineralizing animals evolve and late Ediacaran taxa (e.g., *Cloudina*) reach a global distribution.

Methods

Samples were collected at the Jiulongwan section along a fresh road cut and were marked on the outcrop so that future samples can be positioned precisely relative to the stratigraphic column.

Carbonate Carbon and Oxygen Isotopes ($\delta^{13}C_{carb}$ and $\delta^{13}O_{carb}$). For carbonate carbon and oxygen isotope analysis, powders were microdrilled from the finest-grained portions of polished slabs determined by petrographic observations. Approximately 100 μg of carbonate powder was reacted for 10 min at 90°C with anhydrous H_3PO_4 in a GV Multiprep inlet system connected to a GV Isoprime dual-inlet mass spectrometer. Isotopic results are expressed in the standard δ notation as per mil (‰) deviations from Vienna-PeeDee belemnite. Uncertainties determined by multiple measurements of National Bureau of Standards (NBS)-19 were better than 0.05‰ (1σ) for both C and O isotopes. Analyses were carried out at the University of Maryland and Institute of Arctic and Alpine Research, University of Colorado. Parallel analyses were carried out at the Institute of Geology and Geophysics, Chinese Academy of Sciences, by using conventional off-line extraction techniques and a Finnigan MAT 252 mass spectrometer. Oxygen isotope compositions were not corrected for dolomitic samples.

Organic Carbon Isotopes ($\delta^{13}C_{org}$) and Abundance. Organic carbon abundance and isotope data were determined following the procedures in ref. 7. Approximately 1 g of whole rock powder was weighed and then acidified with 6 M HCl. Residues were washed with deionized H_2O, centrifuged, dried, and weighed to determine carbonate abundance. Total organic carbon abundance was calculated by using the percent carbonate data and measured abundance of carbon in the residues quantified by elemental analysis. Isotope abundances were measured on a continuous-flow GV Isoprime mass spectrometer at University of Maryland and a Finnigan MAT 252 at the Institute of Geology and Geophysics. $\delta^{13}C_{org}$ values are reported as per mil (‰) deviations from Vienna-PeeDee belemnite. Uncertainties based on multiple analyses of a standard carbonate are better than 0.12% (1σ) for total organic carbon and 0.5‰ (1σ) for $\delta^{13}C_{org}$.

Pyrite Sulfur Isotopes ($\delta^{34}S_{py}$) and Concentrations. Pyrite concentrations and isotopic compositions were analyzed by using both combustion and chromium reduction methods (49). Organic-rich samples typically contained enough pyrite for direct elemental analyzer combustion analysis of decalcified residues. For samples with low total organic carbon concentrations, powdered samples were reacted with 50 ml of 1 M $CrCl_2$ and 20 ml of 10 M HCl in an N_2 atmosphere. H_2S produced from pyrite reduction by $CrCl_2$ was bubbled through a 1 M zinc-acetate trap, precipitated as ZnS, and converted to Ag_2S by ion exchange with $AgNO_3$. The Ag_2S was centrifuged, washed, dried, and weighed.

Pyrite sulfur isotopes and concentrations were determined by elemental analyzer combustion at 1030°C on a continuous-flow GV Isoprime mass spectrometer. Decalcified residue (100–500 μg) or Ag_2S (100 μg) was dropped into a quartz reaction tube packed with quartz chips and elemental Cu for quantitative oxidation and O_2 resorption. Water was removed with a 10-cm magnesium perchlorate trap, and SO_2 was separated from other gases with an 0.8-m polytetrafluoroethylene GC column packed with Porapak 50–80 mesh heated at 90°C. Pyrite concentrations were calculated from SO_2 yields. $\delta^{34}S_{py}$ values are reported as per mil (‰) deviation from Vienna-Canyon Diablo triolite. Uncertainties determined from multiple analyses of NBS-127 interspersed with the samples are better than 0.3% (1σ) for concentration and 0.3‰ (1σ) for isotope composition.

Parallel $\delta^{34}S_{py}$ data were analyzed by using a conventional off-line combustion method (≈15 mg of Ag_2S and 150 mg of V_2O_5 were combusted at 1050°C for 15 min) and a dual-inlet Delta S mass spectrometer at the Institute of Geology and Geophysics.

CAS Concentrations and Isotopes ($\delta^{34}S_{CAS}$). CAS extraction was conducted by using techniques modified from refs. 50 and 51. Approximately 100 g of fresh sample was powdered and treated with 30% hydrogen peroxide for 48 h to remove nonstructurally bound sulfate and organic sulfur that might contaminate CAS (T. Lyons, personal communication). Leached powders were dissolved in 3 M HCl, and insoluble residues were separated from the supernatant by filtration through 8-μm Whatman filters. Ten ml of 0.1 M $BaCl_2$ was added to 40 ml of supernatant to precipitate barite. Precipitates were centrifuged, washed, dried, and weighed.

CAS concentrations were calculated from inductively coupled plasma atomic emission spectrometer analysis of small aliquots of the leached solutions at the Virginia Tech Soil Testing Laboratory. CAS concentrations were

calculated from sulfur abundances and reported as parts per million of SO_4^{2-} (±5%). Barite precipitates were combusted with a Eurovector elemental analyzer, and $^{34}S/^{32}S$ ratios were determined by using a continuous-flow GV Isoprime mass spectrometer at the University of Maryland. A conventional off-line combustion method and a Delta S mass spectrometer were used for barite analysis at the Institute of Geology and Geophysics. $\delta^{34}S_{CAS}$ values are reported as per mil (‰) deviation from Vienna-Canyon Diablo triolite. Uncertainties determined from multiple analyses of NBS-127 are better than 0.2‰ (1σ).

ACKNOWLEDGMENTS. We thank T. Lyons and P. Hoffman for constructive comments. This work was supported by the National Science Foundation, the National Science Foundation of China, the National Aeronautics and Space Agency, the Geological Society of America, the American Association of Petroleum Geologists, the Paleontological Society, the Chinese Academy of Sciences, the Chinese Ministry of Science and Technology, Virginia Tech Institute of Critical Technology and Applied Sciences, the Evolving Earth Foundation, Deutsche Forschungsgemeinschaft, and Westfälische Wilhelms-Universität Münster.

1. Kaufman AJ, Jacobsen SB, Knoll AH (1993) The Vendian record of Sr and C isotopic variations in seawater: Implications for tectonics and paleoclimate. *Earth Planet Sci Lett* 120:409–430.
2. Hoffman PF, Kaufman AJ, Halverson GP, Schrag DP (1998) A Neoproterozoic snowball Earth. *Science* 281:1342–1346.
3. Knoll AH, Carroll SB (1999) Early animal evolution: Emerging views from comparative biology and geology. *Science* 284:2129–2137.
4. Fike DA, Grotzinger JP, Pratt LM, Summons RE (2006) Oxidation of the Ediacaran ocean. *Nature* 444:744–747.
5. Canfield DE, Poulton SW, Narbonne GM (2007) Late Neoproterozoic deep-ocean oxygenation and the rise of animal life. *Science* 315:92–95.
6. Zhou C, Xie G, McFadden K, Xiao S, Yuan X (2007) The diversification and extinction of Doushantuo–Pertatataka acritarchs in South China: Causes and biostratigraphic significance. *Geol J* 42:229–262.
7. Kaufman AJ, Corsetti FA, Varni MA (2007) The effect of rising atmospheric oxygen on carbon and sulfur isotope anomalies in the Neoproterozoic Johnnie Formation, Death Valley USA *Chem Geol* 237:47–63.
8. Yin L, *et al.* (2007) Doushantuo embryos preserved inside diapause egg cysts. *Nature* 446:661–663.
9. Halverson GP, Hurtgen MT (2007) Ediacaran growth of the marine sulfate reservoir. *Earth Planet Sci Lett* 263:32–44.
10. Waggoner B (2003) The Ediacaran biotas in space and time. *Integr Comp Biol* 43:104–113.
11. Condon D, *et al.* (2005) U-Pb ages from the Neoproterozoic Doushantuo Formation, China. *Science* 308:95–98.
12. Jiang G, Kennedy M, Christie-Blick N, Wu H, Zhang S (2006) Stratigraphy, sedimentary structures, and textures of the late Neoproterozoic Doushantuo cap carbonate in South China. *J Sediment Res* 76:978–995.
13. Hoffman PF, *et al.* (2007) Are basal Ediacaran (635 Ma) postglacial ''cap dolostones'' diachronous? *Earth Planet Sci Lett* 258:114–131.
14. Yin C, Bengtson S, Yue Z (2004) Silicified and phosphatized *Tianzhushanian*, spheroidal microfossils of possible animal origin from the Neoproterozoic of South China. *Acta Palaeontol Pol* 49:1–12.
15. Xiao S, Yuan X, Steiner M, Knoll AH (2002) Macroscopic carbonaceous compressions in a terminal Proterozoic shale: A systematic reassessment of the Miaohe biota, South China. *J Paleontol* 76:347–376.
16. Ding L, *et al.* (1996) *Sinian Miaohe Biota* (Geological Publishing House, Beijing).
17. Tang F, Yin C, Liu Y, Wang Z, Gao L (2006) Discovery of macroscopic carbonaceous compression fossils from the Doushantuo Formation in eastern Yangtze Gorges. *Chin Sci Bull* 50:2632–2637.
18. Sun W (1986) Late Precambrian pennatulids (sea pens) from the eastern Yangtze Gorge, China: *Paracharnia* gen. nov. *Precambrian Res* 31:361–375.
19. Xiao S, Shen B, Zhou C, Xie G, Yuan X (2005) A uniquely preserved Ediacaran fossil with direct evidence for a quilted bodyplan. *Proc Natl Acad Sci USA* 102:10227–10232.
20. Weber B, Steiner M, Zhu MY (2007) Precambrian–Cambrian trace fossils from the Yangtze Platform (South China) and the early evolution of bilaterian lifestyles. *Palaeogeogr Palaeoclimatol Palaeoecol* 254:328–349.
21. Chen Z, Bengtson S, Zhou C, Hua H, Yue Z (2008) Tube structure and original composition of *Sinotubulites*: Shelly fossils from the late Neoproterozoic in southern Shaanxi, China. *Lethaia* 41:37–45.
22. Zhang Y, Yin L, Xiao S, Knoll AH (1998) Permineralized fossils from the terminal Proterozoic Doushantuo Formation, South China. *J Paleontol* 72 (Suppl):1–52.
23. Zhou C, Xiao S (2007) Ediacaran $\delta^{13}C$ chemostratigraphy of South China. *Chem Geol* 237:89–108.
24. Marenco PJ, Corsetti FA, Hammond DE, Kaufman AJ, Bottjer DJ (2008) Oxidation of pyrite during extraction of carbonate associated sulfate. *Chem Geol* 247:124–132.
25. Rothman DH, Hayes JM, Summons R (2003) Dynamics of the Neoproterozoic carbon cycle. *Proc Natl Acad Sci USA* 100:8124–8129.
26. Jiang G, Kennedy MJ, Christie-Blick N (2003) Stable isotopic evidence for methane seeps in Neoproterozoic postglacial cap carbonates. *Nature* 426:822–826.
27. Shields GA (2005) Neoproterozoic cap carbonates: A critical appraisal of existing models and the plumeworld hypothesis. *Terra Nova* 17:299–310.
28. Higgins JA, Schrag DP (2003) Aftermath of a snowball Earth. *Geochem Geophys Geosys*, 10.1029/2002GC000403.
29. Zhu M, Zhang J, Yang A (2007) Integrated Ediacaran (Sinian) chronostratigraphy of South China. *Palaeogeogr Palaeoclimatol Palaeoecol* 254:7–61.
30. Jiang G, Kaufman AJ, Christie-Blick N, Zhang S, Wu H (2007) Carbon isotope variability across the Ediacaran Yangtze platform in South China: Implications for a large surface-to-deep ocean $\delta^{13}C$ gradient. *Earth Planet Sci Lett* 261:303–320.
31. Wang Z, Yin C, Gao L, Liu Y (2002) Chemostratigraphic characteristics and correlation of the Sinian stratotype in the eastern Yangtze Gorges area, Yichang, Hubei Province. *Geol Rev* 48:408–415.
32. Wang W, *et al.* (2002) Isotopic chemostratigraphy of the upper Sinian in Three Gorges area. *Acta Micropalaeontol Sin* 19:382–388.
33. Barfod GH, *et al.* (2002) New Lu-Hf and Pb-Pb age constraints on the earliest animal fossils. *Earth Planet Sci Lett* 201:203–212.
34. Kah LC, Lyons TW, Frank TD (2004) Low marine sulphate and protracted oxygenation of the Proterozoic biosphere. *Nature* 431:834–838.
35. Hurtgen MT, Arthur MA, Halverson GP (2005) Neoproterozoic sulfur isotopes, the evolution of microbial sulfur species, and the burial efficiency of sulfide as sedimentary pyrite. *Geology* 33:41–44.
36. Kendall B, Anbar AD, Gordon G, Arnold GL, Creaser RA (2006) Constraining the redox state of the Proterozoic deep oceans using the Mo isotope systematics of euxinic black shales. *Geol Soc Am Abstr Prog* 38(7):56.
37. Li R, *et al.* (1999) Spatial and temporal variations in carbon and sulfur isotopic compositions of Sinian sedimentary rocks in the Yangtze Platform, South China. *Precambrian Res* 97:59–75.
38. Xiao S, Zhang Y, Knoll AH (1998) Three-dimensional preservation of algae and animal embryos in a Neoproterozoic phosphorite. *Nature* 391:553–558.
39. Hua H, Chen Z, Yuan X, Zhang L, Xiao S (2005) Skeletogenesis and asexual reproduction in the earliest biomineralizing animal *Cloudina*. *Geology* 33:277–280.
40. Kaufman AJ, Jiang G, Christie-Blick N, Banerjee DM, Rai V (2006) Stable isotope record of the terminal Neoproterozoic Krol platform in the Lesser Himalayas of northern India. *Precambrian Res* 147:156–185.
41. Corsetti FA, Kaufman AJ (2003) Stratigraphic investigations of carbon isotope anomalies and Neoproterozoic ice ages in Death Valley, California. *Geol Soc Am Bull* 115:916–932.
42. Jiang G, Sohl LE, Christie-Blick N (2003) Neoproterozoic stratigraphic comparison of the Lesser Himalaya (India) and Yangtze block (south China): Paleogeographic implications. *Geology* 31:917–920.
43. Le Guerroue E, Allen PA, Cozzi A, Etienne JL, Fanning M (2006) 50 Myr recovery from the largest negative $\delta^{13}C$ excursion in the Ediacaran ocean. *Terra Nova* 18:147–153.
44. Walter MR, Veevers JJ, Calver CR, Gorjan P, Hill AC (2000) Dating the 840–544 Ma Neoproterozoic interval by isotopes of strontium, carbon, and sulfur in seawater, and some interpretative models. *Precambrian Res* 100:371–433.
45. Gorjan P, Veevers JJ, Walter MR (2000) Neoproterozoic sulfur-isotope variation in Australia and global implications. *Precambrian Res* 100:151–179.
46. Calver CR (2000) Isotope stratigraphy of the Ediacarian (Neoproterozoic III) of the Adelaide Rift Complex, Australia, and the overprint of water column stratification. *Precambrian Res* 100:121–150.
47. Halverson GP, Dudás FÖ, Maloof AC, Bowring SA (2007) Evolution of the $^{87}Sr/^{86}Sr$ composition of Neoproterozoic seawater. *Palaeogeogr Palaeoclimatol Palaeoecol* 256:103–129.
48. Grey K (2005) Ediacaran palynology of Australia. *Memoirs Assoc Australasian Palaeontol* 31:1–439.
49. Canfield DE, Raiswell R, Westrich JT, Reaves CM, Berner RA (1986) The use of chromium reduction in the analysis of reduced inorganic sulfur in sediments and shale. *Chem Geol* 54:149–155.
50. Burdett J, Authur M, Richardson M (1989) A Neogene seawater sulfur isotope age curve from calcareous pelagic microfossils. *Earth Planet Sci Lett* 94:189–198.
51. Gellatly AM, Lyons TW (2005) Trace sulfate in mid-Proterozoic carbonates and the sulfur isotope record of biospheric evolution. *Geochim Cosmochim Acta* 69:3813–3829.